Soft Matter

Self-assembly of lobed particles into amorphous and crystalline porous structures

Journal:	*Soft Matter*
Manuscript ID	SM-COM-09-2019-001878.R1
Article Type:	Communication
Date Submitted by the Author:	28-Nov-2019
Complete List of Authors:	Paul, Sanjib; university of new hampshire Vashisth, Harish; University of New Hampshire, Chemical Engineering

Soft Matter

ARTICLE TYPE

Cite this: DOI: 00.0000/xxxxxxxxxx

Self-assembly of lobed particles into amorphous and crystalline porous structures†

Sanjib Paul[a] and Harish Vashisth *[a]

Received Date
Accepted Date

DOI: 00.0000/xxxxxxxxxx

We report simulation studies on the self-assembly of hard-lobed particles (patchy particles where patches appear as lobes around a seed) of different shapes and show that various types of self-assembled morphologies can be achieved by tuning inter-lobe interactions. On self-assembly, the linear building blocks having two lobes around the seed formed rings, the trigonal planar building blocks formed cylindrical hollow tubes and two-dimensional sheets, and the square planar building blocks formed spherical clathrates. The tetrahedral, trigonal bipyramidal, and the octahedral-shaped particles formed compact porous crystalline structures which are constituted by either hexagonal close packed or face centered cubic lattices. The pore size distributions revealed that linear, trigonal planar, and square planar building blocks create highly porous self-assembled structures. Our results suggest that these self-assembled morphologies will potentially find applications in tissue engineering, host-guest chemistry, adsorption, and catalysis.

Colloidal patchy particles have gained importance due to their ability to self-assemble into higher-order structures (colloidal molecules, colloidal polymers, and even colloidal crystals) dictated by their shapes and directional interactions[1–7]. Based upon the structures and chemical functionalities, these self-assembled entities have potential applications as photonic band gap materials[8], catalysts,[9] and biomaterials[10,11]. Notwithstanding challenges in the controlled synthesis of patchy particles, several synthesis techniques have been devised[12–16] and applied to demonstrate, for example, self-assembly of spherical triblock Janus particles into a two-dimensional kagome lattice.[17] A staged self-assembly process in which different patches are sequentially activated was further shown to form porous structures as well as cubic diamond and body centered cubic lattices.[18,19] Not only the spherical particles, non-spherical patchy particles (where patches appear as lobes around a central seed) have been shown to self-assemble into colloidal molecules and polymers.[20] Moreover, soft patchy particles made up of terpolymers were shown to form long colloidal polymers by self-assembly or co-assembly between different types of building blocks.[21]

Although non-spherical patchy particles of different shapes can be synthesized, detailed investigations on their self-assembled morphologies are yet to be carried out. A molecular simulation study on the self-assembly of spherical patchy particles revealed that structures like chains, sheets, tetrahedra, and icosahedra can be obtained depending on the number and location of patches on the spherical surface.[22] We hypothesized that if patches appear as hard lobes and are positioned at specific locations to design specific particle-shapes, then the self-assembly of those particles may lead to higher-order structures. Moreover, directional interactions between the hard lobes will create more excluded volume around each particle because of their non-spherical shape that may lead to porous self-assembled structures.

In this work, we have studied the self-assembly of different types of hard-lobed particles into porous morphologies. Specifically, we have chosen lobed particles ($S^m_{N_L}$, m denotes the shape and N_L denotes the number of lobes present in the particle) as building blocks of seven different shapes (Fig. 1): snowman (S^{SM}_1), dumbbell (S^{DB}_2), trigonal planar (S^{TP}_3), square planner (S^{SP}_4), tetrahedral (S^{TH}_4), trigonal bipyramidal (S^{TBP}_5), and octahedral (S^{OCT}_6). The shapes of lobed particles considered in this study are experimentally realizable[20,23–25]. For example, Stefano et al.[23] synthesized single to multi-lobed particles of different shapes by first nucleating oil droplets (3-methacryloxypropyl trimethoxysilane oligomers) around negatively charged polystyrene seeds and then solidifying the oil droplets using the radical polymerization technique. Meester et al.[25] have also shown a way of producing lobed particles of defined shapes by reconfiguring the random aggregates of spherical colloids.

[a] Department of Chemical Engineering, University of New Hampshire, 33 Academic Way, Durham, NH 03824, USA; E-mail: harish.vashisth@unh.edu

† Electronic Supplementary Information (ESI) available: [Details on simulation models and methods, a table, and ten figures are included.]

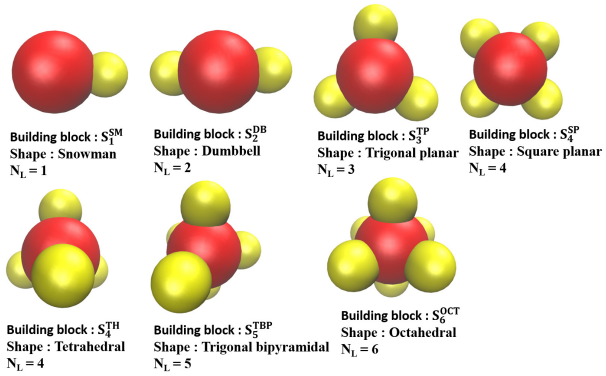

Fig. 1 Seven building blocks of different shapes are shown in space-filling representations. The central seed (C) and the lobes (L) are represented by red and yellow spheres, respectively.

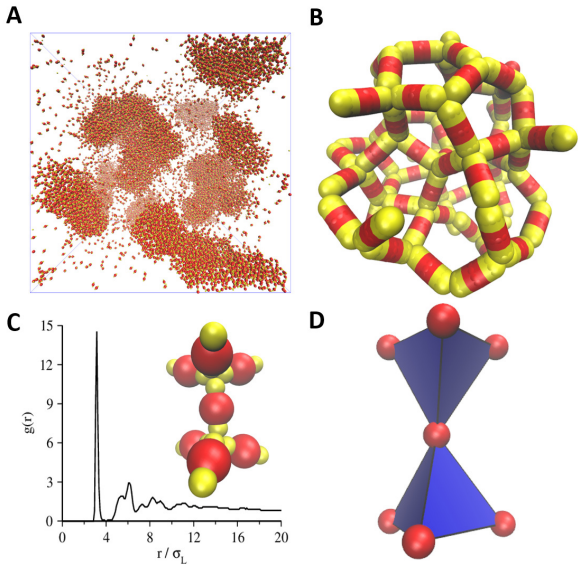

Fig. 2 Self-assembly of S_2^{DB} building blocks: (A) Simulation domain showing the formation of self-assembled structures at $\tilde{\varepsilon}_{LL} = 7.5$, (B) Ring structures formed by the building blocks, (C) Radial distribution function for the C-C pair; (inset) A snapshot of the first coordination shell of a building block, and (D) Trigonal prismatic geometry of the seeds in the first coordination shell.

For each building block, we have performed coarse-grained Langevin dynamics simulations using the GPU-accelerated software HOOMDBlue.[26,27] The non-bonded interactions between the lobes are attractive and have been modeled by the Lennard-Jones potential and the interactions between two central seeds (C) and also between a lobe (L) and a seed (C) are repulsive and have been modeled by the surafce-shifted Lennard-Jones potential implemented in HOOMD-BLue (see supplemental methods, ESI†). For each building block, we have tuned the parameter ε_{LL}/k_BT (ε_{LL} is the depth of potential well for the L-L pair, k_B is the Boltzmann constant, and T is the temperature), which we denote by $\tilde{\varepsilon}_{LL}$ (reduced interactions between the lobes in k_BT units), to observe its effect on the self-assembly. The $\tilde{\varepsilon}_{LL}$ values employed in this work are 3.0, 3.8, 4.3, 5.0, 6.0, 7.5. We also carried out simulations with multiple initial configurations to test the robustness of self-assembled structures obtained, as has been done in previous studies[28]. We further report the convergence of potential energy per particle vs. simulation time (Fig. S1, ESI†).

We have observed that the occurrence of self-assembly depends on the number of lobes (N_L) and the non-bonded interactions ($\tilde{\varepsilon_{LL}}$). In the case of S_6^{OCT}, the lowest $\tilde{\varepsilon}_{LL}$ value that shows self-assembly is 3.8, but the lowest $\tilde{\varepsilon}_{LL}$ value showing self-assembly increases as the number of lobes decreases (Table S1, ESI†). The S_1^{SM} building blocks with one lobe do not show self-assembly for any $\tilde{\varepsilon}_{LL}$ value. The S_2^{DB} building blocks exhibit self-assembly only at $\tilde{\varepsilon}_{LL} = 7.5$. Since the building blocks in all simulations have attractive interactions only through the lobes, a higher number of lobes around a seed creates a higher number of sites of attraction and thereby results in their self-assembly at a lower $\tilde{\varepsilon}_{LL}$ value. For each system, we further estimated the change in averaged potential energy per particle (E_p) with the change of $\tilde{\varepsilon}_{LL}$ or reduced temperature, T^* (Fig. S2, ESI†). In each case, we observed a sharp change in E_p when the lobed particles undergo transitions from disordered states to self-assembled states, a feature of the first order transitions. Such transitions have also been observed in the self-assembly of spherical patchy particles with four patches at four equatorial positions or two ring patches near the poles that were found to undergo first order transitions from disordered phases to self-assembled two dimensional sheets or icosahedra[22]. We now describe key structural features of various self-assembled morphologies.

For S_1^{SM} building blocks, we did not observe self-assembly for $\tilde{\varepsilon}_{LL}$ values ranging between 3.0 and 7.5 (Table S1, ESI†). We then tested their self-assembly at a higher value ($\tilde{\varepsilon}_{LL} = 15.0$) and found that S_1^{SM} particles form small triangular planar or tetrahedral clusters (Fig. S3, ESI†). The S_2^{DB} building blocks showed self-assembled clusters at $\tilde{\varepsilon}_{LL} = 7.5$ (Fig. 2A and Table S1, ESI†). The clusters were found to be constituted by 5, 6, and 7 membered rings (Fig. 2B) which is different from the self-assembled structures (chains) obtained for the spherical patchy particles having two surface patches at two opposite poles[22], instead of lobes. The radial distribution function (RDF) calculated for the C-C pair reveals that long range order is not present in these clusters, thereby indicating the formation of amorphous structures, where the building blocks located in a bulk cluster are surrounded by six other building blocks. The first coordination shell (inset in Fig. 2C) shows that the central seed (with respect to which the first coordination shell is computed), along with the seeds from neighboring building blocks, forms a trigonal prismatic geometry (Fig. 2D).

For S_3^{TP} building blocks, we observed self-assembled structures at $\tilde{\varepsilon}_{LL} = 6.0$ and 7.5 (Table S1). At $\tilde{\varepsilon}_{LL} = 6.0$, building blocks self-assemble to form long porous cylindrical tubes and many such interconnected tubes of different diameters and lengths further organize into larger tubular assemblies (Fig. 3A, B and Fig. S4A and S4B, ESI†). The length and the width of the longest and widest tube detected are 36 σ_L (length; σ_L is lobe diameter) and 8 σ_L (width), respectively. The RDF computed for the C-C pair reveals no long range order in the cluster (Fig. 3C and Fig. S4C, ESI†). The first coordination shell for a building block deeply

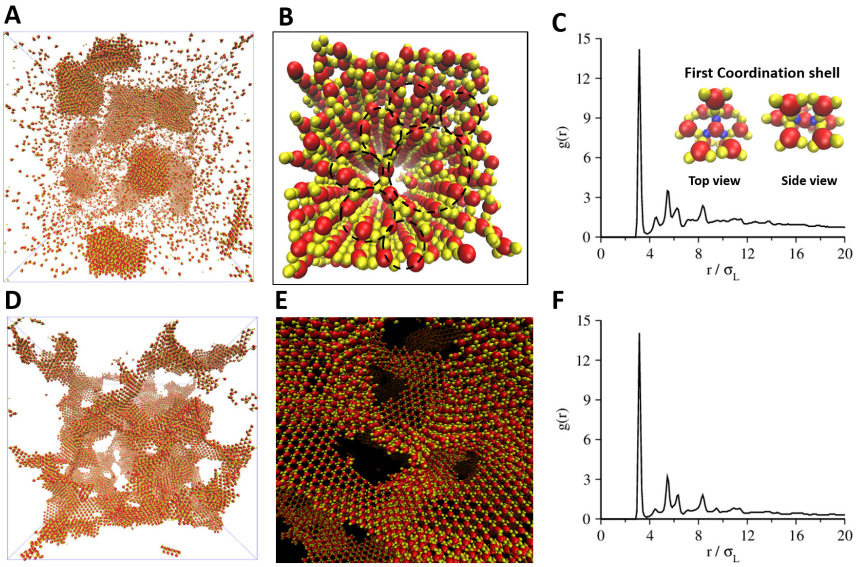

Fig. 3 Self-assembly of S_3^{TP} building blocks: (A) Simulation domain showing the formation of self-assembled structures, (B) A cuboid extracted from the cluster showing the tubes of different diameters (the open ends of a few tubes are highlighted by black dotted circles), (C) Radial distribution function for the C-C pair; (inset) the first coordination shell of a building block is shown with the lobes of the central building block highlighted in blue, (D) Simulation domain showing the formation of two dimensional sheets at $\tilde{\varepsilon}_{LL} = 7.5$, (E) A zoomed-view of the simulation domain showing the formation of two dimensional sheets, and (F) Radial distribution function computed for the C-C pairs present in two-dimensional sheets.

buried in the cluster is shown in the inset of Fig. 3C highlighting that each of the three lobes of S_3^{TP} building blocks is attached with three other lobes from three different building blocks and thus each building block is surrounded by 9 other building blocks in its first coordination shell. However, at $\tilde{\varepsilon}_{LL} = 7.5$, S_3^{TP} building blocks self-assemble to form porous two-dimensional sheet-like structures (Fig. 3D). In these structures, each of the three lobes is attached with 2 other lobes from 2 different building blocks and thereby each building block is surrounded by 6 other building blocks in its first coordination shell and long range order is absent (Fig. 3E, F).

For $S4_4^{SP}$ and $S4_4^{TH}$, the building blocks formed polyhedron-shaped structures at $\tilde{\varepsilon}_{LL} = 5.0$ (Fig. 4A and 5A). The square planar building blocks ($S4_4^{SP}$), unlike their spherical analogues (spherical patchy particles having four surface patches at four equatorial positions that self-assemble into two-dimensional sheets[22]), were observed to self-assemble into close packed spherical clathrates (Fig. 4B and Fig. S4E, ESI†). Each spherical clathrate was comprised of 12 building blocks where the seed in each building block occupies the vertices of a cuboctahedron (Fig. 4C). The RDF calculated for the C-C pair shows multiple intense peaks depicting that higher order structures are embedded within the self-assembled morphologies (Fig. 4D and Fig. S4F, ESI†). The coordination number for a building block is 10 (inset snapshot in Fig. 4D).

Unlike $S4_4^{SP}$, the $S4_4^{TH}$ building blocks do not self-assemble into spherical clathrates but they are well-ordered inside the self-assembled structures as revealed by the RDF (Fig. 5B). The first coordination shell displayed in Fig. 5B (inset) shows that each of the four lobes of the central tetrahedral building block is attached with three lobes from three different building blocks and hence surrounded by 12 other building blocks. Twelve seeds belonging to 12 building blocks present in the first coordination shell and the central seed with respect to which the first coordination shell is measured form hexagonal close packed structures constituted by two different kinds of planes (Fig. 5C). At higher $\tilde{\varepsilon}_{LL}$, both S_4^{SP} and S_4^{TH} building blocks self-assemble to form porous wire-like structures (Fig. S5A and S5B, ESI†) and at very high $\tilde{\varepsilon}_{LL}$ ($\tilde{\varepsilon}_{LL} = 15.0$), S_4^{SP} building blocks formed two-dimensional sheet like structures (Fig. S6, ESI†).

The trigonal bipyramidal (S_5^{TBP}) and the octahedral (S_6^{OCT}) building blocks formed compact polyhedron shaped self-assembled structures at $\tilde{\varepsilon}_{LL} = 4.3$ and 3.8, respectively (Fig. 5D, G). For both of these systems, multiple peaks present in the RDF (Fig. 5E, H) indicate that the building blocks are highly ordered and correlated in these self-assembled structures. The number of building blocks in the first coordination shell is 12 for both S_5^{TBP} and S_6^{OCT}. The first coordination shell for S_5^{TBP} and S_6^{OCT} shows that the building blocks are tightly packed in these systems (inset in Fig. 5E, H). For S_5^{TBP}, the seeds are arranged in hexagonal close packed structures comprised of two different planes similar to S_4^{TH} (Fig. 5C, F), but for S_6^{OCT}, the seeds are organized as face centered cubes which are constituted by three different types of planes (Fig. 5I). With an increase in $\tilde{\varepsilon}_{LL}$, the shapes of these self-assembled structures became gradually thinner and longer and at very high $\tilde{\varepsilon}_{LL}$, they formed long extended structures (Fig. S5D and S5F, ESI†).

We further characterized porous assemblies by computing the distributions of pore diameters (Fig. 6A) using the Zeo++ software[29,30] by extracting the largest possible cuboids (Fig. S7, ESI†) from self-assembled structures. The pore-diameter distributions show that each building block produces a sharp peak (except S_2^{DB} and S_3^{TP}) showing uniform pore-sizes. However, the self-assembled structures obtained from S_2^{DB} have pores with larger

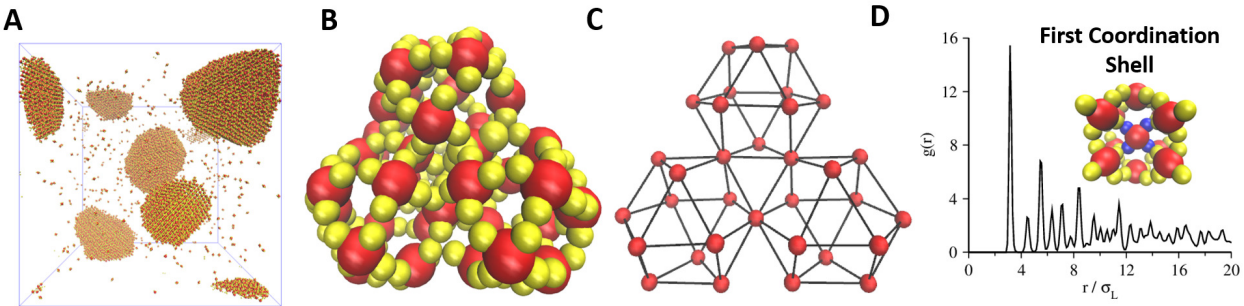

Fig. 4 Self-assembly of S_4^{SP} building blocks: (A) Simulation domain showing the formation of polyhedron shaped self-assembled structures at $\tilde{\epsilon}_{LL} = 5.0$, (B) Structures of spherical clathrates formed by the S_4^{SP} building blocks, (C) Hexagonal close packing of self-assembled cuboctahedrons; the red spheres are the seeds of the lobed particles, (D) Radial distribution function for the C-C pair; the presence of multiple peaks indicates the formation of crystalline structures; (inset) the first coordination shell of a building block is shown with the lobes of the central building block highlighted in blue.

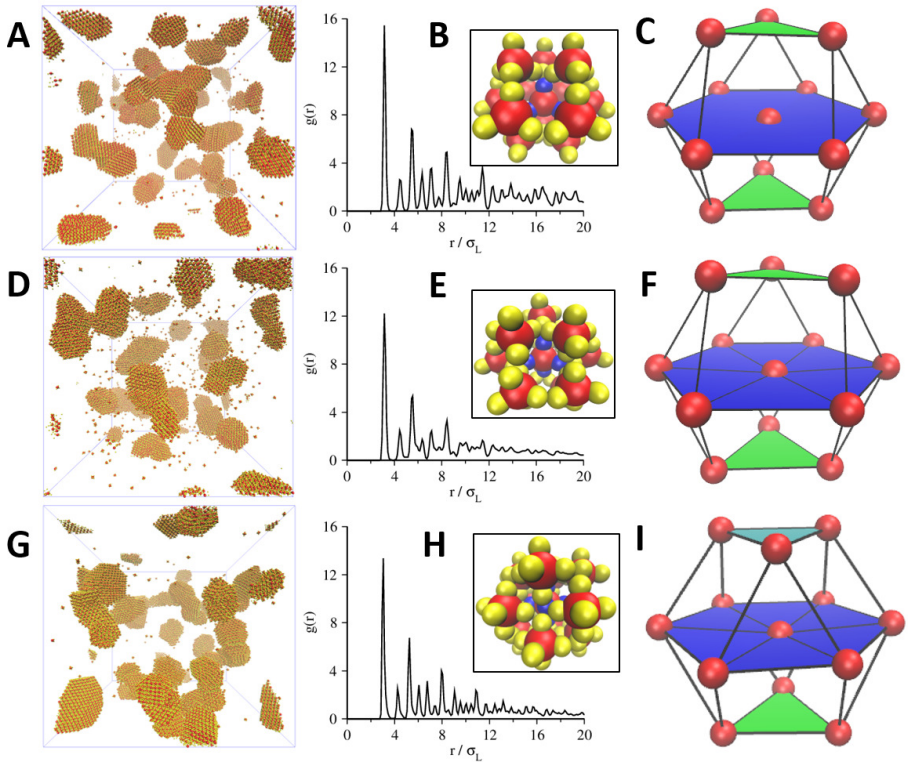

Fig. 5 Snapshots and data corresponding to self-assembly of S_4^{TH} (panels A, B, C), S_5^{TBP} (panels D, E, F), and S_6^{OCT} (panels G, H, I) building blocks: (A, D, G) Simulation domains showing the formation of many polyhedron shaped clusters; (B, E, H) RDFs show the presence of multiple peaks indicating the formation of crystalline structures, and the first coordination shells (inset); the lobes of the central particles with respect to which the first coordination shell were measured are depicted in blue; (C and F) Hexagonal close packed structures comprised of two different planes *a* (green) and *b* (blue); and (I) Face centered cubic lattice comprised of three different planes *a* (cyan), *b* (blue) and *c* (green) formed by the seeds of 13 lobed particles (12 in the first coordination shell and 1 in the center).

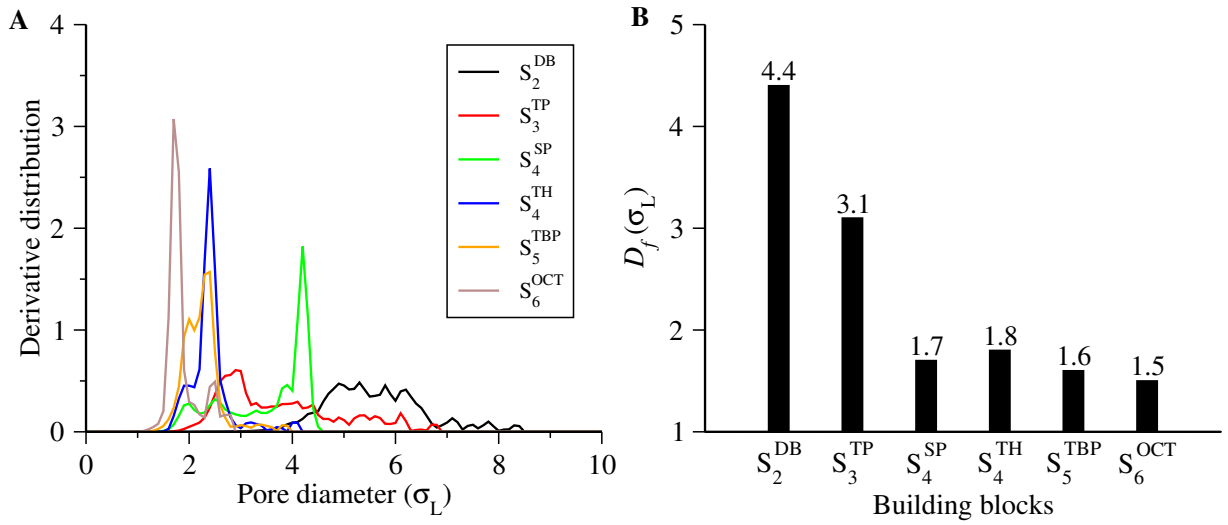

Fig. 6 (A) Derivative distributions of the pore volume, and (B) the diameter (D_f) corresponding to the largest free sphere present in the self-assembled structures.

diameters ranging between $4\sigma_L$ to $8\sigma_L$ due to the presence of large rings. Similarly, for S_3^{TP}, a wider pore-diameter distribution is observed with values ranging between $2\sigma_L$ to $7\sigma_L$. This pattern of the pore-size distribution can be attributed to the fact that S_3^{TP} building blocks self-assemble into cylindrical hollow tubes of different diameters. The S_4^{SP} building blocks also show larger pore-sizes (as indicated by a sharp peak at $\sigma_L = 3.9$) which is due to the formation of spherical clathrates. The pore diameters for the S_4^{TH} and S_5^{TBP} building blocks are nearly identical. The self-assembled structures based upon S_6^{OCT} lead to the smallest pores likely due to a tighter packing given the maximum number of lobes. We also estimated the diameter of the largest free sphere (D_f; Fig. 6B), the largest sphere that can freely move within the self-assembled porous structures. Consistent with the pore-diameter distributions, these data show that D_f is maximum for S_2^{DB} building blocks, which is followed by S_3^{TP}. This is due to the presence of ring structures obtained from S_2^{DB} building blocks and interconnected tubes from S_3^{TP}. For the remaining cases, the values of D_f are smaller and comparable.

To understand the effect of density of particles on the self-assembled structures, we performed simulations of several types of lobed particles (dumbbell, trigonal planar, square planar and trigonal bipyramid) at different volume fractions ($\phi = 0.01$ to 0.11). For different ϕ values, we calculated the number of self-assembled clusters formed at the end of simulations and also calculated the percentage of the number of building blocks present in each self-assembled cluster using the depth first search algorithm[31]. We observed that at very low volume fractions ($\phi =$ 0.01), the lobed particles do not self-assemble on simulation timescales of 10^8 steps (Fig. S8, ESI†). However, at higher volume fractions ($\phi = 0.05$ to 0.11), the lobed particles self-assemble into larger clusters (Fig. S9, ESI†) but the local arrangement of the lobed particles in final self-assembled morphologies does not change on increasing the density (Fig. S10, ESI†).

In conclusion, we have tested the self-assembly of lobed particles of seven different shapes and shown that lobed particles can self-assemble into higher order porous structures if the inter-lobe interactions are tuned. We show that not only the patch size,[20] interactions between the patches (lobes) also determine the number of particles in the first coordination shell. At lower $\tilde{\varepsilon}_{LL}$, the dumbbell and the triangular planar (S_3^{TP}) shaped building blocks form highly porous amorphous structures. At lower $\tilde{\varepsilon}_{LL}$, the triangular building blocks are surrounded by 9 other building blocks and form cylindrical hollow tubes, but at higher $\tilde{\varepsilon}_{LL}$, they are surrounded by 6 building blocks to form two-dimensional sheets. Given these self-assembled morphologies, trigonal planar building blocks can be compared with the sp^2 hybridized carbon atoms which form carbon nanotubes and graphene sheets in two allotropic states. The square planar S_4^{SP} building blocks self-assembled into close packed spherical clathrates at lower $\tilde{\varepsilon}_{LL}$. Each spherical clathrate is constituted by 12 building blocks and the seeds of these 12 building blocks are located at the vertices of a cuboctahedron. The S_4^{TD}, S_5^{TBP} and S_6^{OCT} building blocks self-assembled into very compact structures with smaller pore-sizes. The S_4^{TD} and S_5^{TBP} building blocks were also observed to assemble in a hexagonal close packing arrangement, and the S_6^{OCT} building blocks into face centered cubic lattices.

The self-assembly study carried out in this work is scale independent and therefore it is applicable to particles of sub-micrometer to micrometer sizes. Gong et al.[24] have recently proposed a method called colloidal fusion to synthesize spherical patchy particles of different sizes. This method does not rely on the chemistry of particles but rather on a simple physico-chemical algorithm incorporating symmetry and composition information. Therefore, the method can produce patchy particles from *nm* to μm sizes. Pine and coworkers[20] have also designed a method where the clusters of microspheres are first made using the emulsion-evaporation technique and then a two-stage swelling process followed by polymerization is performed to produce patchy lobed particles of different shapes. To our knowledge, the lobed particles synthesized so far are primarily designed with non-biodegradable polymers like polystyrene, which may

not be suitable for biomedical applications, where biodegradable polymers are likely needed. Since the dumbbell-shaped particles generate larger and well-connected pores in self-assembled morphologies reported in this work, we surmise that these particles, if designed in the micron-size range and using biodegradable polymers, could be useful to mimic the extracellular matrix[32]. The three lobed planar particles of nanometer size can also be used as building blocks to prepare synthetic channels for applications in molecular separations. If the interactions between the lobes are tuned, these particles can also self-assemble in two-dimensional sheets with likely applications in adsorption and catalysis[33]. The four lobed planar particles are likely useful to study host-guest chemistry as they are capable of creating clathrate-like structures. We suggest that findings from this work will inspire future experimental work aimed at exploring the self-assembly of lobed particles of various sizes.

Acknowledgements

We are grateful for financial support provided by the National Science Foundation (award No. OIA-1757371; HV). We acknowledge computational support through the following resources: Premise, a central shared HPC cluster at UNH supported by the Research Computing Center; BioMade, a heterogeneous CPU/GPU cluster supported by the NSF EPSCoR award (OIA-1757371; HV); and the NSF-supported (ACI-1548562) Extreme Science and Engineering Discovery Environment (XSEDE)[34] Comet resource at San Diego Supercomputer Center (SDSC) under grant TG-MCB160183 (HV). We also thank Dr. Maciej Haranczyk for discussions on pore-size distributions.

Conflicts of Interest

There are no conflicts to declare.

Notes and references

1 P. F. Damasceno, M. Engel and S. C. Glotzer, *Science*, 2012, **337**, 453–457.
2 S. C. Glotzer and M. J. Solomon, *Nat. Mater.*, 2007, **6**, 557–562.
3 I. C. Pons-Siepermann and S. C. Glotzer, *ACS Nano*, 2012, **6**, 3919–3924.
4 S. Ravaine and E. Duguet, *Curr. Opin. Colloid Interface Sci*, 2017, **30**, 45 – 53.
5 F. Li, D. P. Josephson and A. Stein, *Angew. Chem. Int. Ed*, 2011, **50**, 360–388.
6 T. Oh, S. S. Park and C. A. Mirkin, *Advanced Materials*, 2019, **31**, 1805480.
7 H. Lin, S. Lee, L. Sun, M. Spellings, M. Engel, S. C. Glotzer and C. A. Mirkin, *Science*, 2017, **355**, 931–935.
8 Y. Xia, B. Gates and Z.-Y. Li, *Adv. Mater.*, 2001, **13**, 409–413.
9 Z. W. Seh, S. Liu, M. Low, S.-Y. Zhang, Z. Liu, A. Mlayah and M.-Y. Han, *Adv. Mater.*, 2012, **24**, 2310–2314.
10 H.-J. Zhai, B. Kiran, B. Dai, J. Li and L.-S. Wang, *J. Am. Chem. Soc*, 2005, **127**, 12098–12106.
11 S. Tsonchev, G. C. Schatz and M. A. Ratner, *Nano Lett.*, 2003, **3**, 623–626.
12 J.-G. Park, J. D. Forster and E. R. Dufresne, *J. Am. Chem. Soc.*, 2010, **132**, 5960–5961.
13 V. N. Manoharan, M. T. Elsesser and D. J. Pine, *Science*, 2003, **301**, 483–487.
14 P. M. Johnson, C. M. van Kats and A. van Blaaderen, *Langmuir*, 2005, **21**, 11510–11517.
15 J.-W. Kim, R. Larsen and D. Weitz, *Adv. Mat.*, 2007, **19**, 2005–2009.
16 J. Yuan, L. Wang, L. Zhu, M. Pan, W. Wang, Y. Liu and G. Liu, *Langmuir*, 2015, **31**, 4087–4095.
17 Q. Chen, S. C. Bae and S. Granick, *Nature*, 2011, **469**, 381–.
18 Q. Chen, S. C. Bae and S. Granick, *J. Am. Chem. Soc.*, 2012, **134**, 11080–11083.
19 D. Morphew, J. Shaw, C. Avins and D. Chakrabarti, *ACS Nano*, 2018, **12**, 2355–2364.
20 Y. Wang, Y. Wang, D. R. Breed, V. N. Manoharan, L. Feng, A. D. Hollingsworth, M. Weck and D. J. Pine, *Nature*, 2012, **491**, 51.
21 K. H. Ku, Y. Kim, G.-R. Yi, Y. S. Jung and B. J. Kim, *ACS Nano*, 2015, **9**, 11333–11341.
22 Z. Zhang and S. C. Glotzer, *Nano Lett.*, 2004, **4**, 1407–1413.
23 S. Sacanna, M. Korpics, K. Rodriguez, ColÃşn-MelÃĺndez, K. Laura, Seung-Hyun, D. J. Pine and G.-R. Yi, *Nat. Commun*, 2013, **4**, 1688–.
24 Z. Gong, T. Hueckel, G.-R. Yi and S. Sacanna, *Nature*, 2017, **550**, 234.
25 V. Meester, R. W. Verweij, C. van der Wel and D. J. Kraft, *ACS Nano*, 2016, **10**, 4322–4329.
26 J. A. Anderson, C. D. Lorenz and A. Travesset, *J. Comp. Phys.*, 2008, **227**, 5342 – 5359.
27 J. Glaser, T. D. Nguyen, J. A. Anderson, P. Lui, F. Spiga, J. A. Millan, D. C. Morse and S. C. Glotzer, *Comput. Phys. Commun*, 2015, **192**, 97 – 107.
28 Zhang, M. A. Horsch, M. H. Lamm and S. C. Glotzer, *Nano Letters*, 2003, **3**, 1341–1346.
29 M. Pinheiro, R. L. Martin, C. H. Rycroft and M. Haranczyk, *CrystEngComm*, 2013, **15**, 7531–7538.
30 M. Pinheiro, R. L. Martin, C. H. Rycroft, A. Jones, E. Iglesia and M. Haranczyk, *J. Mol. Graph. Model*, 2013, **44**, 208 – 219.
31 R. Tarjan, *SIAM J. Comput*, 1972, **1**, 146–160.
32 Q. L. Loh and C. Choong, *Tissue Engineering Part B: Reviews*, 2013, **19**, 485–502.
33 C. Perego and R. Millini, *Chem. Soc. Rev.*, 2013, **42**, 3956–3976.
34 J. Towns, T. Cockerill, M. Dahan, I. Foster, K. Gaither, A. Grimshaw, V. Hazlewood, S. Lathrop, D. Lifka, G. D. Peterson, R. Roskies, J. R. Scott and N. Wilkins-Diehr, *Comput. Sci. Eng.*, 2014, **16**, 62–74.

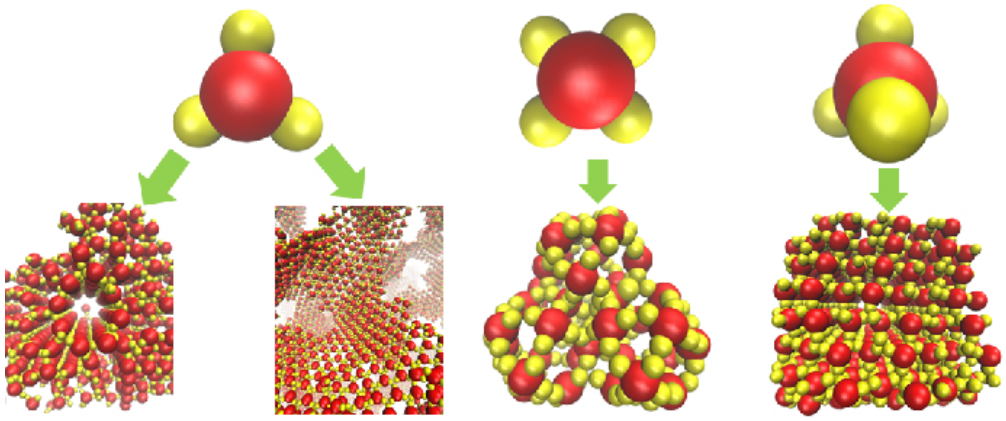

175x73mm (100 x 100 DPI)